ADVANCED FUNCTIONAL MATERIALS
www.afm-journal.de

Smectic Liquid Crystalline Titanium Dioxide Nanorods: Reducing Attractions by Optimizing Ligand Density

Seyed Naveed Hosseini, Albert Grau-Carbonell, Anna G. Nikolaenkova, Xiaobin Xie, Xiaodan Chen, Arnout Imhof, Alfons van Blaaderen,* and Patrick J. Baesjou**

Crystalline titanium dioxide (TiO_2) semiconductor nanorods (NRs) feature several optical properties, such as birefringence combined with high refractive indexes and a wide bandgap precluding optical absorption in visible-light spectrum, making them attractive for many applications such as optoelectronics. Dispersing these NRs in suitable solvents creates inorganic liquid crystals (LCs) offering enhanced collective and orientation-dependent properties, which can additionally be utilized to manipulate optical behavior. Herein, a synthetic procedure from literature is scaled up and coupled with an important post-synthesis-treatment step such that self-assembled NRs dried onto a liquid interface and in bulk can be investigated. Comprehensive characterizations confirm the vital role of surface ligand density of the NRs in reducing the effects of attractions between them and thus increasing the range of volume fractions in which these dispersions can be exploited. Various symmetries (hexagonal or tetragonal) can be achieved in the smectic layers of NRs by tuning the aspect ratios of the NRs from 4.8 to 8.5. Experiments show that external fields such as shear flow or electric fields can easily either induce a reversible nematic order in isotropic dispersions or order existing LC phases over much longer regions, opening many opportunities to manipulate light for optical applications.

1. Introduction

Anisotropic colloidal particles have many properties different from spherical particles that can be exploited in different crystal and liquid crystalline phases that form by self-assembly (SA).[1–5] Liquid crystals (LCs) formed by inorganic anisotropic particles demonstrate tunable optical characteristics that are of great interest for optical and optoelectronic devices.[6–8] In addition to analogous properties exhibited by LCs formed by small molecules, inorganic LCs can be utilized not only as a model system to investigate molecular interactions and LC formation,[9–12] but can also greatly benefit from intrinsic properties of the dispersed building blocks.[13–16] For instance, nanocrystalline TiO_2 is of interest because of its high refractive indexes, ranging from $n = 2.448$ to $n = 2.947$, a wide band gap, and strong UV absorption combined with low light absorption in the visible-light spectrum.[17,18] In addition, crystalline TiO_2 nanoparticles (NPs) have been shown to be of interest as a (photo)catalyst or as catalyst support in heterogeneous catalysis.[18–22] Therefore, colloidal TiO_2 nanocrystals in different polymorphs have been synthesized through various chemical routes that exert precise control over particle size and shape, and nanorods (NRs) are well-studied among them.[18,20,23–25] In the formation of inorganic LCs from these NRs, attractions caused by van der Waals forces and/or depletion effects are to first order proportional to the particle size and can strongly affect the phase behavior. In recent works from our group, it was shown that spherical nanoparticles with van der Waals attractions that at contact have a magnitude of 0.5 kT with k Boltzmann's constant and T the absolute temperature, crystallized at the same volume fraction of 0.5 as hard spherical particles. However, stronger attractions of 2 kT already decreased the volume fraction to 0.11 and caused the systems to fall out of equilibrium.[26,27] We are interested in using the high refractive indexes of TiO_2 NRs for optical applications, for which it is advantageous if they can be used over as broad range of volume fractions as possible. This can be achieved if the (hard) particle shape dominates the phase behavior, while particle charges and interparticle attractions can be neglected.[28]

In recent years many groups working on the self-assembly of NPs have highlighted the importance of ligands on the interactions between NPs and thus on what type of colloidal (liquid) crystal phases, with different symmetries and interparticle spacings they ultimately form.[29–41] The role of ligands on self-assembly was also recently reviewed.[29] Here we will only mention some typical examples of the role of ligands on SA as discussed in literature and almost all of relevance to the present

S. N. Hosseini, A. Grau-Carbonell, A. G. Nikolaenkova, Dr. X. Xie, X. Chen, Dr. A. Imhof, Prof. A. van Blaaderen, Dr. P. J. Baesjou
Soft Condensed Matter
Debye Institute for Nanomaterials Science
Utrecht University
Princetonplein 5, Utrecht 3584 CC, The Netherlands
E-mail: a.imhof@uu.nl; a.vanblaaderen@uu.nl; p.j.baesjou@uu.nl

The ORCID identification number(s) for the author(s) of this article can be found under https://doi.org/10.1002/adfm.202005491.

DOI: 10.1002/adfm.202005491

paper: Nanocrystals (NCs) have generally different facets with different surface tensions and thus different densities of ligands generally which has been shown to affect the SA behavior of the NPs.[29–32,42] For instance, in ref. [31] the differences in the density of the ligands on different facets of the plate-shaped NPs was determined by density functional calculations by the Glotzer group and the differences that this caused in the interactions between the particles was found to be essential in subsequent simulations of the SA process to explain the colloidal crystal phases as observed by the Murray group. The interparticle distances and thus the interactions are also found to be influenced by the amount of solvent that is still present[33,34] or if an anti-solvent for the ligands is added.[35] The local density of ligands can even be affected by the colloidal crystal phase formed.[32] Excess ligands, even if added after completion of the SA, were also found to be able to affect interparticle spacings and the order in colloidal crystals already formed.[36] It is often the case that ligands are not bound covalently to the surface and thus can be replaced or removed by frequent washing steps[35,42–45] and conversely that the presence of excess ligands affects SA.[36,46] Additionally, addition of excess ligands above the critical micelle concentration can cause the formation of micelles which can induce depletion attractions between the NPs.[46] It is therefore also no surprise that temperature[37,47–49] and even pressure[38] have been shown to affect the ligand interactions and these effects have even been used to improve the order in already assembled colloidal crystals.[37] Varying the core size while keeping the ligands the same also affects the SA and interactions,[33,34,39,40] in such series sometimes the ratio between the core size and ligand length is related to a "softness parameter". Even in such a well-controlled series where core material and ligands are kept the same,[40] there are already many factors changing that may affect the interactions indicating how complex these interactions in general are: Ligand density, which can be a function of the radius of curvature, van der Waals interactions, effective softness. In short, being able to treat the ligand layer as a thin layer that only slightly affects the hard particle size and is simply there to add steep repulsive forces is the exception in the SA of NPs, not the rule.

TiO_2 NPs are typically surface-functionalized with various commercially available alkyl-containing ligands to attain dispersibility in organic solvents.[50] Polymeric surfactants and dendritic macromolecules have also attracted significant attention due to their ability to better mask the strong van der Waals adhesion forces between the NPs and even shapes of the core particles that they are adsorbed onto.[47,51–54] Although polymer-functionalized TiO_2 NPs have been utilized as building blocks for lyotropic LCs, there are a few disadvantages to using these ligands.[48,55,56] First, the synthesis of polymeric ligands adds more complicated steps as they are often not yet available commercially. Furthermore, thick surface coverage by polymeric surfactants on the order of a few nanometers considerably suppresses the effective refractive index of complete particles, which is not desirable for optical applications. Finally, the effective hard aspect ratio is reduced because the interactions between two surfaces with polymers adsorbed to them are generally (much) softer than for shorter ligands like oleylamine (OLAM) or oleic acid (OLAC) as used in this paper.

In this work, TiO_2 NRs were synthesized using a scaled-up version of a literature procedure.[20] We found that a post-synthesis-treatment step designed to fully saturate the surface with ligands reduced attractions and ensured more hard-rod-like phase behavior and thus maintained colloidal stability of the NRs at higher volume fractions in the apolar organic solvents used. The resulting crystalline NRs were mainly composed of the brookite phase of TiO_2 and ranged from almost 27.8 to 83.0 nm in length and 3.4 to 7.0 nm in thickness. Brookite NRs were monodisperse enough that smectic liquid crystal phases of as much as hundreds of layers formed easily both in bulk and onto a liquid interface in 2D. Textures of the LC phases formed in bulk were investigated by polarizing optical microscopy (POM) to identify the phases and these were consistent with what was observed by transmission electron microscopy (TEM) on the liquid interface assembled structures. Preliminary experiments showed that shear and electric fields could easily induce LC behavior in an isotropic NR dispersion and/or align existing NRs' LC phases.

2. Results and Discussion

2.1. Characterization of Synthesized Brookite TiO_2 Nanorods

Figure 1 illustrates the formation of brookite TiO_2 NRs with tunable aspect ratios (short NRs (SNRs), medium NRs (MNRs), and long NRs (LNRs)) achieved through the seeded growth approach from anatase seeds (for details, see **Table 1**, and Modified synthesis method and Nanorods formation mechanism in Supporting Information).

The formation of the anatase seeds and brookite nanorods was confirmed by X-ray diffraction (XRD) analyses and high-resolution transmission electron microscopy (HRTEM) images (Figure 1 and Figures S1–S3, Supporting Information). Presumably, some residual strain remained after the transformation from anatase to brookite, as it was observed in this and previous studies[20,42,57,58] that the synthesized NRs became increasingly bent as their length increased (while still maintaining a single crystalline nature as shown in Figure S2, Supporting Information).

While not mentioned in previous reports, dispersions of as-synthesized brookite NRs, even the smallest, quickly formed gel phases with a yield stress (small bubbles not rising in the dispersion) in any apolar solvent, i.e. hexane, chloroform, or toluene. From these observations and the large discrepancies with expected hard rod-like phase behavior, we inferred that significant attractions between the NRs were responsible for the birefringent gelled states (Figure S4a,b, Supporting Information). Similarly, a surface ligand density as high as possible was found necessary to guarantee crystallization in binary spherical nanoparticles, a process quite sensitive to the presence of attractions between the particles.[43] As it is known that both ligands used here (OLAC and OLAM) do not have extreme bonding strengths,[35,43,44] we have put extra effort in saturating the surfaces of the NRs with additional ligands. Although density functional theory calculations have shown that OLAM plays the most important role in stabilizing {120} planes along the length of the brookite NRs,[42] we observed that OLAM by itself was insufficient. The NRs were synthesized in an excess amount of OLAM and most likely all the potential adsorption sites for OLAM are already occupied. However, those as-synthesized NRs still suffered from remaining attractions. In contrast, we

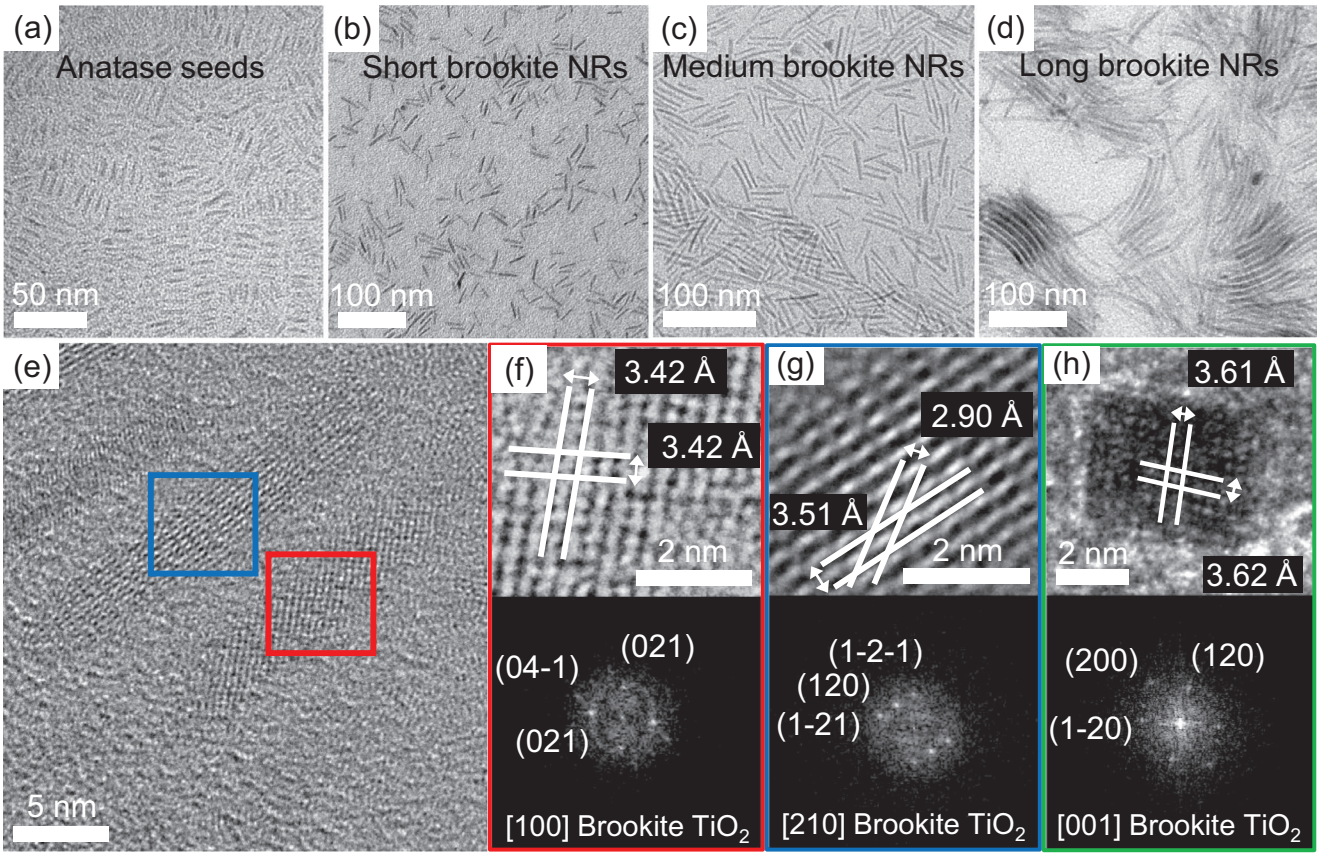

Figure 1. a) Anatase seeds and b–d) various brookite NRs with different aspect ratios (short, medium, long) synthesized by adding different amounts of titanium precursor. e–g) High-resolution TEM micrographs of short TiO_2 NRs with the brookite crystal structure. f,g) The red and blue insets highlight selected areas and their corresponding electron diffraction power spectra (FFT). h) The green inset highlights a selected area containing one medium nanorod standing perpendicular to the image showing a rhomboidal cross-section and its corresponding power spectrum (FFT). In the selected areas of the micrograph, the distance between the identified planes is presented. In the power spectra, the indexed zone axes are displayed.

found that post-treatment with excess OLAC was successful in improving the colloidal stability of the NRs. These post-treated NRs exhibited no gel formation even at high volume fractions (up to 32 vol% in toluene) for SNRs with an aspect ratio of 4.8 and dispersions were stable for months (Figure S4, Supporting Information). We surmise that the main reason that OLAC is more successful than OLAM, is that while both ligands chemisorb to the surface of the nanoparticles, OLAC forms stronger monodentate carboxylate based bonding to surface sites of the transition metal oxide nanoparticles as compared to the (neutral) amine ligands.[45] This is further supported by the observation that post-treatment of the NRs with OLAM did not result in improved stability. After post-treatment thermogravimetric analysis/mass spectrometry (TGA/MS, Figure S5, Supporting Information) showed a clear increase in surface coverage of post-treated compared to as-synthesized SNRs (Table 1). From the weight loss and the average dimensions of the SNRs (L = 27.8 ± 2.6 nm and T = 3.4 ± 0.3 nm), measured from TEM images, the ligand density on the surface of as-synthesized SNRs was found to be around 2.3 molecules per nm^2 (see ligand density calculations in Supporting Information and Figure S5, Supporting Information). Post-treated SNRs had a ligand density of ≈2.7 molecules per nm^2. The difference in ligand density also translated into an almost 1.0 nm larger interparticle spacing of neighboring NRs lying parallel, as observed in TEM images (1.2 ± 0.2 nm as-synthesized SNRs to 2.2 ± 0.3 nm post-treated SNRs). Moreover, the post-treatment raised the temperature at which the ligands were completely decomposed by 47 °C. Hence, the enhanced thermal stability is attributed to a higher ligand density and, in particular, more monodentate bound carboxylates, which ensure higher dispersibility of brookite NRs.[43,45] Therefore, by coupling the post-treatment step with a scaled-up synthesis process, brookite NRs were synthesized which were better ligand capped so that van der Waals forces were better suppressed.

The presence of the vertically oriented brookite NRs imaged on the TEM grid in Figure 1h allowed us to estimate the relevant distances of closest approach for the calculation of van der Waals attractions between the inorganic cores. The cores were parallelepipeds with a square cross-section, for which theoretical expressions are available[59] (see van der Waals interactions calculations in the Supporting Information and Figure S6, Supporting Information). **Figure 2** shows calculated van der Waals interactions between short and medium NRs for three different relative orientations and using the Hamaker constants of anatase and brookite (solid and dashed lines, respectively).

The results clearly show a significantly reduced attraction between the post-treated NRs. The strongest attractions

Table 1. Properties of the systems of TiO_2 NRs used in this work. Here, L is the length of inorganic rods, T the thickness, σ the polydispersity, L/T the hard rod aspect ratio, and $(L/T)_{eff}$ the effective rod aspect ratios (where 3 nm was added to both L and T reflecting twice the length of the ligand molecules).

System	L [nm]	σ_L [%]	T [nm]	σ_T [%]	L/T	$(L/T)_{eff}$	SA onto an interface (concentrations) [mg mL^{-1}]	Interparticle spacing [nm]	SA in bulk(volume fraction) [%]
SNR	27.4	9.6	3.4	8.7	8.1	4.8	1.0, 4.0, 8.0	As-synthesized: 1.2 ± 0.2 Post-treated: 2.2 ± 0.3 With depletant: 2.7 ± 0.3	(dispersion I)[a] 25% (dispersion II)[b] 32%
MNR	42.2	10.3	5.1	12.0	8.3	5.6	1.0, 4.0, 8.0	As-synthesized: 1.1 ± 0.2 Post-treated: 2.5 ± 0.4 With depletant: 3.6 ± 0.3	–
LNR	82.9	12.6	7.1	12.6	11.7	8.5	–	–	–

[a,b]Dispersion I and II were prepared from as-synthesized and post-treated SNRs, respectively.

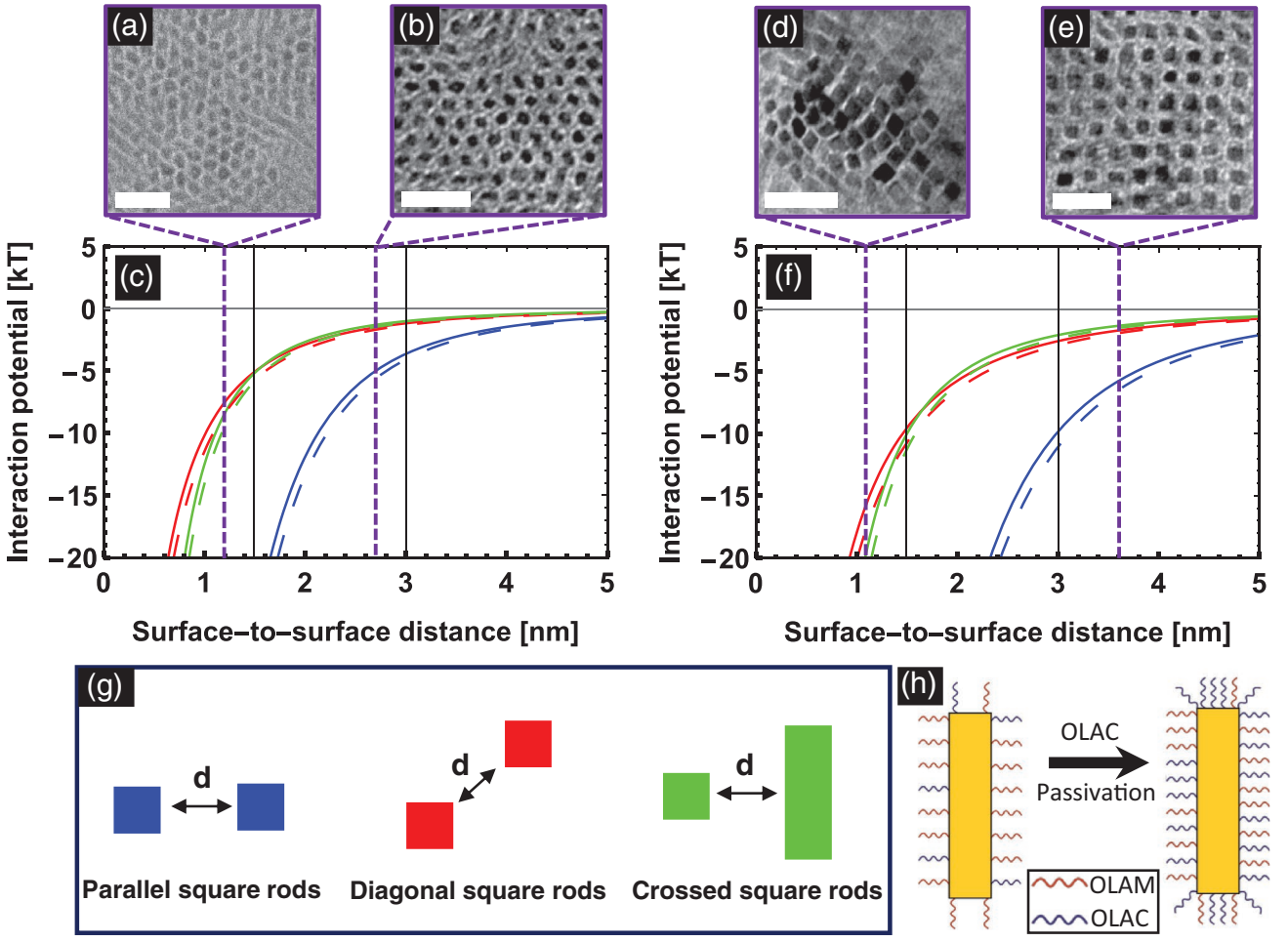

Figure 2. van der Waals interaction potentials between two bare TiO_2 NRs of anatase (solid lines) and brookite (dashed lines) phase, respectively, as well as schematic representation of a single nanorod before and after post-treatment step with OLAC molecules. In (a–c) van der Waals potentials are calculated for short brookite and anatase NRs in which NRs encounter each other in parallel, diagonal, or crossed configuration shown in blue, red, and green colors, respectively. These three configurations are schematically presented with corresponding colors in (g). Two TEM micrographs are presented which show the interparticle distances observed in this study. In (a,b) self-assembled SNRs are displayed for two distinct cases. In (a) as-synthesized SNRs are self-assembled while they are quite attractive. In (b), post-treated SNRs are self-assembled where OLAC has been also introduced as a depletant agent. Panels (d–f) are the same as (a–c) but for MNRs of brookite and anatase. Vertical black solid lines depict one and two times the effective ligand length of 1.5 nm while the vertical purple dashed lines are corresponding to the interparticle spacing observed in the linked TEM images. The reduced spacing in (a,d) could possibly be linked to less ligand coverage around the as-synthesized NRs. h) A sketch of proposed passivation of brookite NRs surface with OLAC molecules. Scale bars in (a,b,d,e) are 20 nm.

occur when rods are perfectly aligned face-to-face, as expected. However, the calculated interactions are an overestimation as they assume perfectly smooth brookite cores with atomically flat interfaces. Any surface roughness would make the "perfect" parallel approach between two rods much less efficient and reduce the actual van der Waals interactions (Figure S2, Supporting Information).[60,61] Additionally, although parallel NRs experience remarkably larger van der Waals attractions, they are rare in an isotropic rod dispersion since the majority of collisions will occur in more or less crossed and/or diagonal orientations resulting in less van der Waals attractions.

2.2. Self-Assembly of Brookite TiO_2 Nanorods into Liquid Crystalline Phases onto a Liquid Interface

In order to investigate the phase behavior of the TiO_2 NRs, the toluene solvent of a dispersion of the NRs was allowed to evaporate, resulting in a self-assembled layer on top of an immiscible water phase. This technique to obtain a monolayer or multilayer assembly of colloidal crystals of NPs was made quite popular by the Murray group.[62,63] It has been shown that the static dielectric constant and surface tension of polar liquids utilized as subphases, can strongly direct the orientation of NCs superlattices formed on the liquid interface.[7,64,65] However, it should be mentioned that depending on the particular NP system, it is also possible that a 2D self-assembled layer also or instead forms on the toluene-air interface. Water, owing to its high polarity, high surface tension, and immiscibility with apolar inorganic solvents like toluene, was found to greatly enhance the formation of large horizontal liquid crystalline structures at the interface (**Figure 3**a,d) (for instance as compared to directly drying of the toluene droplets onto a TEM grid, results not shown). Nonhorizontal configurations of the TiO_2 NRs were formed when OLAC was added to the system, while other parameters that could affect the final morphology such as subphase, temperature, dispersing solvent, and monodispersity were kept the same (Figure 3b,c,e,f). OLAC and other ligands can form micelles above the so-called critical micelle concentration (approximately 0.08 M for OLAC in toluene) during the later stages of the drying process, which can induce depletion attractions between the colloidal NRs (Figure 3).[66,67] Furthermore, these micelles could possibly be adsorbed onto the ligand layers and form "bilayers".[68,69]

Figure 3a,d show smectic LC layers for which the 1D crystalline order lies parallel to the local director of the rods in the plane of the TEM grid. For SA, 40.0 µL of NRs dispersion in toluene (4.0 mg mL^{-1}) was dropcast on to the water subphase (dispersion thickness was around 14.0 µm) and covered with a glass petri dish to slow evaporation. It is highly unlikely that the smectic layers, visible in Figure 3a,d, formed in bulk, but more likely either on the water surface and/or the toluene-air interface. For hard spherocylinders with effective aspect ratios of 4.8 (SNR) and 5.6 (MNR), the nematic to smectic transitions are at packing fractions of 0.50 and 0.47, respectively, although these values are only an indication as they are for idealized monodisperse systems,[28] but the experimental polydispersity, reported in Table 1, modifies the phase behavior.[70–75] As indicated in Figure 3d and Figure S7b,c, Supporting Information, defects such as edge dislocations, splay distortions, domains perpendicularly positioned with respect to the other layers, and point defects (e.g., interstitial NRs lying or standing between lamellae as transverse interlayer particle[74,76] or foreign differently shaped nanoparticles trapped as inclusions) can be observed. At lower concentrations of both SNRs and MNRs (1.0 mg mL^{-1}), only short-ranged local smectic ordered layers with the rods parallel to the grid were observed (Figure S7d, Supporting Information). However, interestingly, by increasing the NR concentration up to 8.0 mg mL^{-1}, regions of vertically aligned NRs were found among horizontally aligned smectic layers. These were ordered occasionally with hexagonal symmetry or randomly packed similarly to structures observed for smectic-A phases (Figure S7e,f, Supporting Information). Although we cannot presently prove this, we think it is likely that the vertically aligned layers were nucleated in bulk and were then oriented with the particles perpendicular to the TEM grids and liquid interface.

Based on the shape of the inorganic core of the brookite NRs, we also investigated the role of the core shape on the ordering inside the smectic layers; examples of which can be seen in Figure 1h and Figure S7g, Supporting Information. Brookite NRs are parallelepipeds growing along [001] direction while they are confined between {120} facets. Therefore, a rhomboidal shape could be recognized as the brookite core cross-section when the rods were imaged standing up on the TEM grid. The observed interparticle spacing for post-treated SNRs was around 2.2 nm, which was less than twice the length of the capping molecules (≈3.0 nm). This spacing is a lower boundary as we assume the nanorods are standing perfectly straight and exactly parallel. If either of these conditions is not met, the projected distance becomes less than the actual local distance between the brookite surfaces. Nevertheless, the ligand shell was still relatively long in comparison with the diameter of these SNRs, giving them approximately a spherocylinder shape when the "cloaking" effect of the softer ligand shell is taken into account and hence superlattices with hexagonal symmetry formed.[51] It is worth noting that if these had been truly hard/sharp parallelepipeds then different close-packed structures would be predicted.[77] We observed (Figure 1 and Table 1) that during the size tuning step, not only do these parallelepipeds grow longitudinally, but they also become slightly thicker. Therefore, we investigated if this thicker core influences the symmetry in the smectic layers. As expected, at a higher concentration for the MNR system, small bundles of vertically aligned MNRs formed with a tetragonal symmetry, because the thickness of the MNRs cores was almost 1.5 times larger compared to the SNRs making the effective cross section of the MNRs much more square (Figure 3g). The interparticle spacing was around 2.5 nm (see Figure S7h, Supporting Information, and Table 1), but because this is a projected distance it is a lower limit of the local distances between the NRs.

In earlier SA experiments that were performed with a similar NR system on an ethylene glycol interface, it was found that SA into regularly structured smectic and smectic-like arrangements was only found to occur when an excess of OLAC was present in the NR dispersion.[78] This was attributed to a depletion-induced attraction that was necessary to induce SA. This is contrary to our finding using a water surface and is also not what is expected, as SA into smectic phases will also

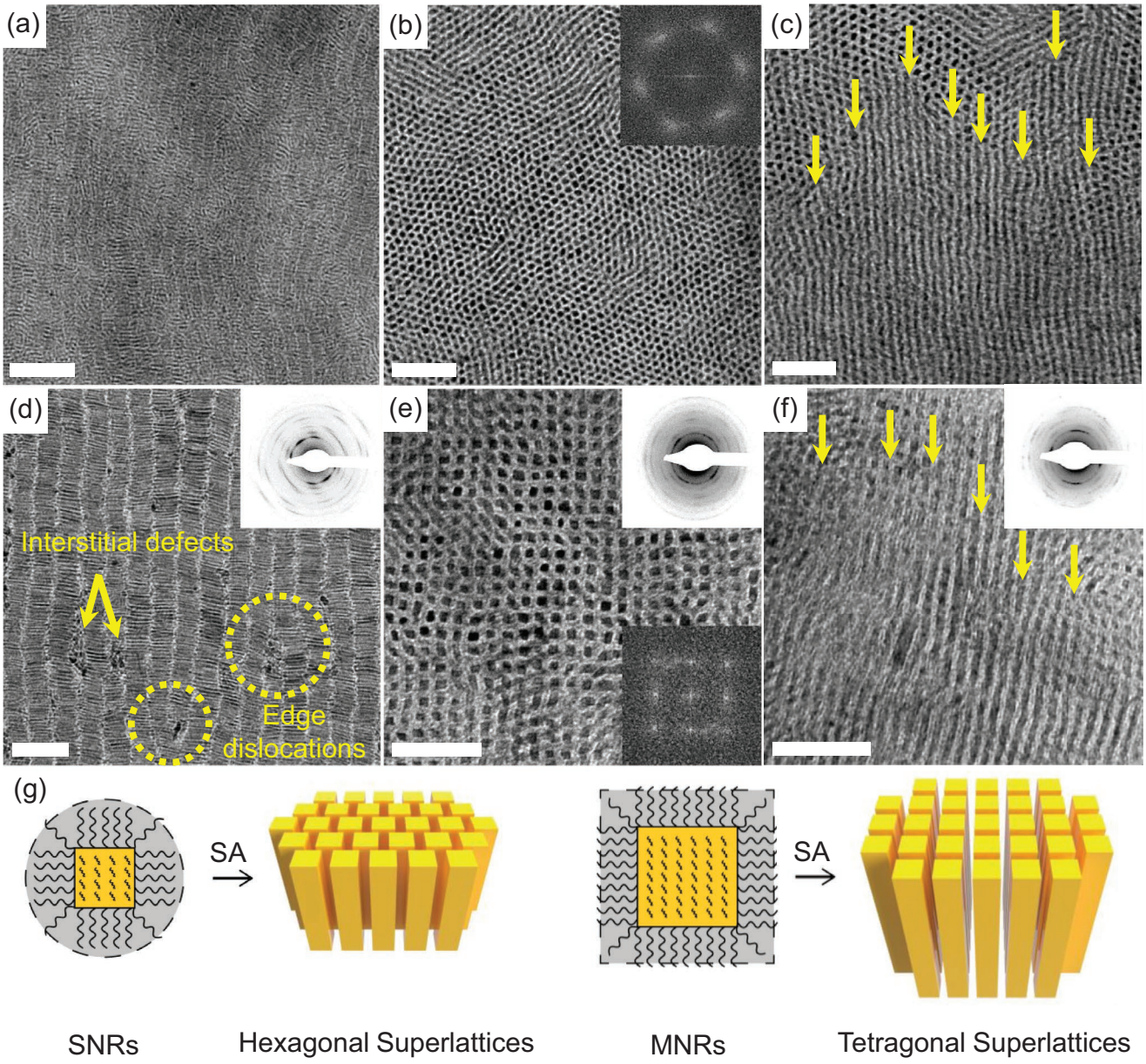

Figure 3. TEM micrographs of short and medium brookite NRs self-assembled at a liquid/air interface. a) Short NRs in a large smectic liquid crystalline domain formed without adding depletant. b,c) Hexagonal superlattices of vertically aligned short NRs formed with added OLAC. Inset in (b) shows the corresponding FFT pattern. In (c) NRs have a tilted orientation, similar to rows of fallen dominoes (yellow arrows). d) Medium NRs in a large smectic liquid crystalline domain formed without adding depletant, demonstrating crystalline structural defects such as edge dislocations and interstitial defects. e,f) Medium NRs vertically aligned in tetragonal superlattices (see the corresponding FFT in (e)) with expanded ligand shell due to the addition of OLAC and formation of the bilayer at the NRs surface. f) Tilted rods are observed in medium NRs similar to short NRs. g) A sketch of proposed effective shape and aspect ratio and resulting influence on stable hexagonal superlattices for SNRs and tetragonal superlattices for MNRs. Scale bars in (a,d) are 100 nm and in (b,c,e,f) 50 nm.

occur with more-or-less hard rods, except at higher volume fractions. Nevertheless, we studied the effect of OLAC micelles on the SA for our rods and observed large self-assembled structures with maximum packing density and hexagonal and tetragonal symmetries for SNR and MNR systems, respectively (Figure 3b,e). However, there were noticeable increases in the interparticle spacings: 2.7 and 3.6 nm for the SNR and MNR systems, respectively, where the values for post-treated NRs without excess OLAC ligands were 2.2 and 2.5 nm, respectively. The excess OLAC ligand molecules clearly expanded the ligand shell around the NRs. Thus, the softness of these NRs increased. Nevertheless, the hard core for the MNR system was still found to determine a tetragonal symmetry in the smectic layers standing perpendicular to the TEM grids. This fact was also observed in simulations for hard parallelepipeds.[69] Under the same experimental circumstances where vertically oriented

self-assembled NRs were found, some large domains of slightly tilted structures were always observed, similar to rows of dominoes fallen into a certain direction, which were also found in the literature before (Figure 3e,f).[46,66,78] Also, several other structures of interest were sometimes spotted such as overlapping bilayers of upstanding NRs with unique patterns, different vortexes, and linear "rail-track" structures which are commonly observed in inorganic LCs and can be observed with their details in Figure S7, Supporting Information.[7,79]

2.3. Liquid Crystalline Phase Behavior in Bulk

To examine the formation of various liquid crystalline phases in bulk, two dispersions were investigated (see Table 1): 1) Dispersion I from as-synthesized SNRs (≈25 vol%) and 2) dispersion II from post-treated SNRs (≈32 vol%). Both dispersions were prepared from SNRs with an effective aspect ratio of 4.8 in which the effective ligand length of 1.5 nm was taken into account.

For dispersion I, the gel formation became evident from ≈4.5 vol% upward due to insufficient surface passivation of the NRs. A gentle shaking of this sample still could induce a transient birefringence, seen with the sample between crossed polarizers (Figure S4b, Supporting Information), indicating that shear induced alignment and relaxation to an isotropic state were still possible. Although at low volume fractions dispersion I exhibited flow birefringence with relatively fast relaxation times up to a few seconds, at higher volume fractions (nearly 25 vol%) the dispersion was highly viscous and relaxation became very slow (on the order of a few days). In literature, it has been observed that heating may increase the stabilizing effect of ligand layers also for rod-like systems.[47–49] We similarly found that by increasing the temperature to around 65 °C dispersion I underwent the nematic to isotropic transition. **Figure 4**a–c shows POM images of dispersion I sheared between two glass slides.

Large brightly birefringent domains with typical nematic Schlieren textures are clearly observed. Transmitted light is completely blocked when the sample is oriented at 45° with respect to the polarizer axis (Figure 4a–c). The orientation, size and direction of domains with a locally similar orientation could simply be manipulated by applying rotational or uniaxial shear forces with shear rates applied on the order of half a second. As a result of rotational shear forces, a large disclination defect with strength +1, seen by 4 dark radial brushes (Figure 4a), annealed out the strain caused by the shear stress via bending the nematic director around.[79] As presented in Figure 4i, we also performed preliminary measurements using an external electric field (2.5 V μm^{-1}, 1 kHz). Such a field could induce a nematic LC phase reversibly in an isotropic liquid dispersion of the SNRs in dispersion II at 32 vol%, thus creating a para nematic phase (see Movie in Supplementary Information). It was also possible to affect the direction of the LC director in dispersion I (25 vol%) where the gelled rest state was already a nematic. A full study of the phase behavior of this titania based LC forming model system will be presented in an upcoming paper with a focus on optical applications of this tunability.

In dispersion II with an initial concentration of 32 vol% we observed equilibrium phase behavior reminiscent of that of hard rods as a result of post treatment of the rods (Figure 4d–h). Dispersion II was initially in an isotropic fluid state and was optically transparent as is expected for hard spherocylinders with an aspect ratio of 4.8 (Figure S4c,d, Supporting Information). Figure 4d shows a POM image of the capillary after resting vertically for 15 days and demonstrates how the formation of a sedimentation equilibrium affected the phase behavior.[80] When the increased diffusional flux upwards created by the osmotic pressure increase balances the settling flux, an equilibrium concentration profile has formed in the gravitational field.[74,80,81] Although the unequivocal assignment of the various LC phases visible requires more detailed characterization techniques such as small-angle X-ray scattering, here different types of LC phases were identified based upon comparing their LC textures to the predictions of computer simulations on the phase behavior of hard rods.[28,62,71,73,74] As shown in Figure 4e, nematic droplets, also known as tactoids, were seen to nucleate and freely float in the isotropic phase in the upper part of the capillary.[82] Owing to their anisotropic surface tension these tactoids were initially quite elongated with a fairly large aspect ratio of around 4.0 and thus almost needle-like with lengths less than 5 μm. Most of these gradually changed into prolate (Figure 4h), a typical tactoid exhibited a uniform change from bright to perfect extinction when rotated from 45° to 0° relative to either of the polarizers, indicating that the tactoid was homogeneous with a uniform director field.[82] Further down, the volume fraction was higher and coalescence of the tactoids and formation of a biphasic region can be seen (Figure 4f). These elongated domains, nearly similar to chains of multiple tactoids, primarily showed nematic-like textures. During the tactoids' growth by coalescence, the elongated domains altered their morphologies resulting in sharp edges and birefringence induced interference colors due to variations in the thicknesses inside the domains. These sharped-edge focal-conic-like patterns are the characteristic texture of smectic.[74,81,83] Eventually, a striated LC texture was distinguished at the lowest part of the capillary belonging to the highest volume fraction which was quite distinctive from the texture of a smectic-A phase (Figure 4f). Based on the observed liquid crystalline structures with hexagonal ordering, two-phase coexistence of smectic-B and crystal at the bottom of the capillary might be still possible (Figure 4g). We surmise that although we have a polydispersity of ≈10% in length of the TiO_2 NRs, length fractionation, and sedimentation-induced macroscopic separation still could provide a possibility to form a crystal phase as well.[73,74] Nevertheless, more detailed XRD studies are required to further investigate the intriguing phase behavior.

3. Conclusion and Outlook

In summary, brookite TiO_2 NRs were synthesized in a scaled-up version of a literature method[20] to such an extent that the liquid crystalline phase behavior of the resulting NRs dispersions could be investigated. These NRs are small enough not to strongly scatter light, but their high refractive indexes and anisotropies can be utilized to manipulate (polarized) light. We

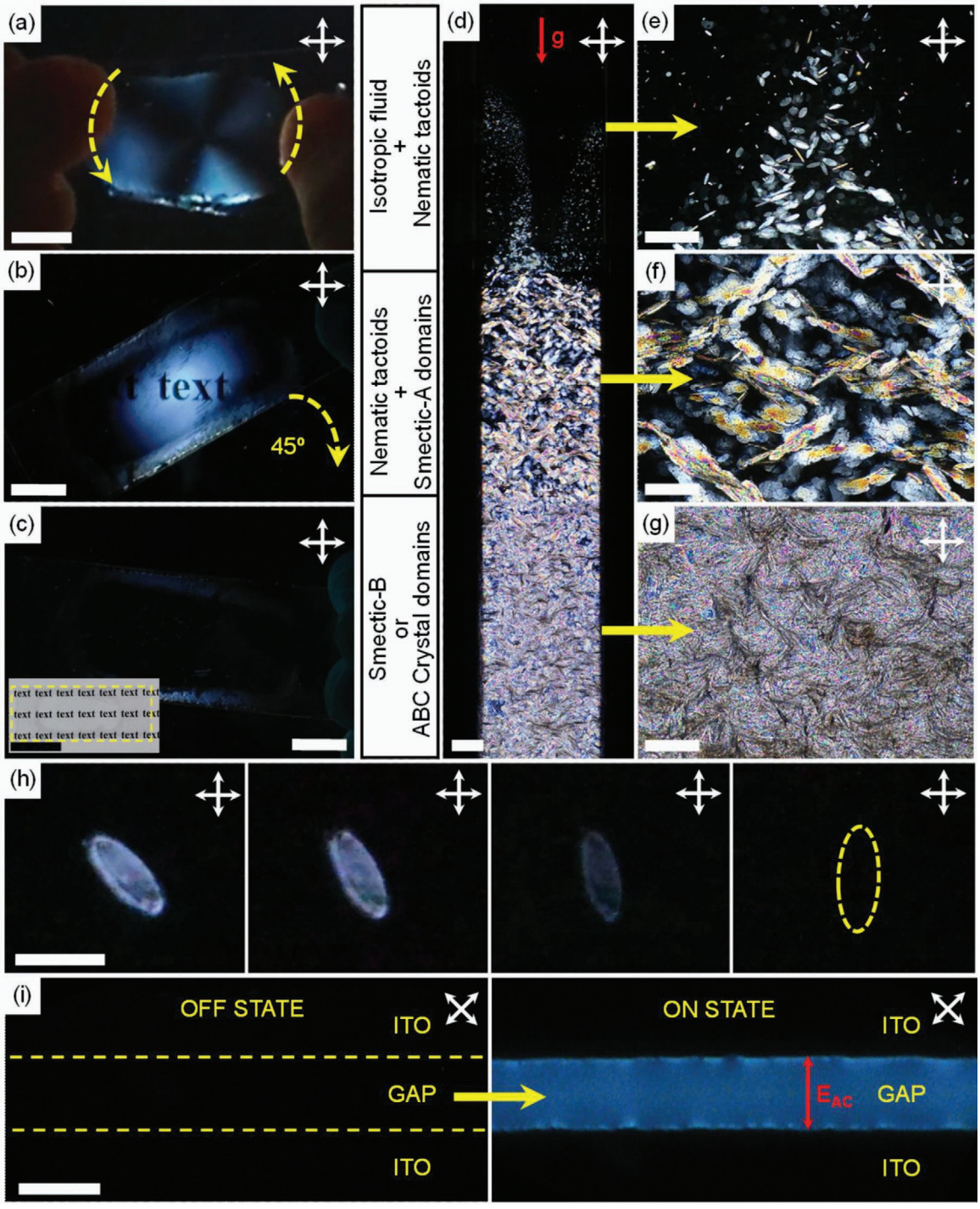

Figure 4. Crossed polarized images of dispersion I and II distinguish between isotropic (dark) and birefringent liquid crystalline phases. a–c) Large bright birefringent domains with typical nematic Schlieren texture from a few droplets of dispersion I placed between two glass slides and viewed between an LCD monitor and a polarizing sheet. The orientation of domains is simply manipulated by applying rotational shear forces (yellow arrows in (a)). and b,c) A large nematic domain completely transmits or blocks light when it is oriented at 45° or 0° with respect to the polarizer axis, respectively. d) A sedimenting sample of dispersion II in a capillary with three distinct regions. From top to bottom: e) homogeneous nematic tactoids floating in isotropic fluid; f) coexistence of nematic tactoids and smectic-A LC phase showing sharped-edge focal-conic Schlieren patterns; g) a striated liquid crystalline texture with the highest packing density belonging to smectic-B and/or crystal phase. h) A typical homogeneous tactoid formed in a sedimenting sample of dispersion II exhibiting a uniform change from the highest brightness to a perfect extinction when it is rotated from 45° to 0° relative to either of the polarizers (in the picture from left to right). i) A large induced nematic-like domain formed from the isotropic dispersion II after an alternating current (2.5 V μm^{-1}, 1 kHz) was applied across a gap in the indium tin oxide (ITO) substrate. Inset in (c) shows that the sample is transparent in unpolarized light. The scale bar in (a,b,c) is 1 cm, in (c-inset) is 2.5 cm, in (d) is 500 µm, in (e,f,g) is 50 µm, in (h) is 10 µm, and in (i) is 150 µm.

investigated various self-assembled liquid crystalline structures formed onto a liquid interface and in bulk by TEM and POM techniques. The NRs were highly crystalline, mainly composed of the brookite phase with tunable aspect ratios between 4.8 and 8.5. Longer brookite NRs were found to become slightly bend (roughly above a length of 50.0 nm and an aspect ratio of 6.0). We found that saturating the brookite NRs interface with OLAC ligand in a post-treatment step was crucial to minimize the detrimental effects of destabilizing attractions between the NRs, which is quite important for use of these systems in applications. Self-assembled structures of the brookite NRs were qualitatively similar to the nematic and smectic liquid crystalline phases predicted for hard rod-shaped particles as the attractions were minimized. Additionally, we could observe that the ordering within the smectic layers could be tuned from hexagonal to tetragonal (which reflects the shape of the brookite cores) by playing with the masking effects of the softer ligand outer layer with respect to the harder core dimensions. Finally, in preliminary experiments on the use of shear or an external electric field we showed that when attractions between the rods were minimized (para) nematic ordering could be reversibly induced in isotropic dispersions, while in dispersions that were already in an LC phase could be also easily oriented and switched. In follow up work we intend to use the possibilities that this nice model system provides in optical applications where the changes in the effective refractive index of the dispersion will be manipulated by external electric fields (e.g. by changing the orientation of the rods and/or the local concentration by (di)electrophoresis). Additionally, we intend to structure these NR LC phases into droplets as well (as we already did earlier with much larger silica rod-based systems also using external electric fields),[84] which would even significantly enlarge the possibilities to arrive at switchable optical devices such as lenses and diffusers.

4. Experimental Section

Materials and Modified Synthesis Method: Monodisperse brookite titanium dioxide (TiO_2) NRs were synthesized following a slightly modified and scaled-up version of the synthesis as described by Murray et al.[18,20] (for details, see Modified synthesis method in Supporting Information).

Post-Treatment of Brookite Nanorods: As-synthesized brookite NRs dispersed in toluene were mixed with OLAC in a 1:5 volume ratio, heated at 75 °C under vacuum, degassed for 15 min, and stirred under nitrogen overnight similar to the literature reported for iron oxide nanoparticles.[43] The resulting NRs were collected by precipitation with the antisolvent ethanol, centrifugation at 8000 rcf for 5 min and re-dispersion in toluene. This post-treatment procedure was repeated twice and ultimately the highly sterically stabilized brookite NRs were re-dispersed in toluene in dilute dispersions. Dispersions with the desired concentration were prepared by careful solvent evaporation. In the case of SNRs, concentrated dispersions of as-synthesized SNRs and post-treated SNRs were referred to dispersion I and dispersion II, respectively. (see Table 1)

Self-Assembly: The liquid interfacial assembly of 2D superlattices was performed by following the procedure as previously described in the literature.[62] In a typical process, brookite NRs from dispersion II in toluene (40.0 µL with concentration of 4.0 mg mL^{-1}) was dropped onto the surface of the water subphase in the glass petri dishes (30.0 mm in diameter and was half-filled with water) and slowly dried by placing a bigger glass petri dish over it. In the case of depletion mediated superlattices, OLAC (5.0 µL) was mixed with brookite NRs dispersion (5.0 µL with concentration of 5.0 mg mL^{-1}) in a vial of toluene (400.0 µL). The mixture was sonicated for 5 min and 40.0 µL of the dispersion was dropcast on the water subphase. Once the NRs dispersion on the interface was fully dried to form the self-assembled layers, resulting films were transferred to carbon-coated 300 mesh copper TEM grids (Agar Scientific). The TEM grids were further dried in a vacuum chamber to remove residuals and used for microscopy analysis. To investigate liquid crystalline textures of self-assembled domains in bulk, a sedimentation experiment was performed as previously reported by Kuijk et al.[74] Briefly, a glass capillary ($0.2 \times 2.0 \times 60.0$ mm^3, Vitrocom) was filled with SNRs from dispersion II with an initial volume fraction of 32%, effective length L = 30.8 nm, diameter D = 6.4 nm, and an aspect ratio of 4.8, in which the ligand length of 1.5 nm was taken into account. Then, the capillary was sealed using a two-component epoxy glue (Bison Kombi rapid) and left vertically to sediment. For dispersion I, at high concentrations (volume fraction of 25%) a highly viscous mixture was observed due to the vdW attractions. Thus, the waxy state was suppressed by heating the sample on a hotplate and dropping the melted mixture between two microscope glass slides to investigate the LC effect by polarizing microscopy.

Characterization: XRD analysis was performed using a Bruker-AXS D2 Phaser X-ray diffractometer with Co Kα radiation (λ = 1.79026 Å) operated at 30 kV and 10 mA. TGA-MS was performed using a PerkinElmer Pyris1 TGA. This technique was utilized to determine the pure inorganic (naked brookite SNRs) loadings and to verify the presence of organic ligands, which contributed to a mass loss at 350–500 °C and specific MS peaks. Two samples (5–10 mg) were prepared from the same batch of SNRs with aspect ratio 4.8, one of had been post-treated. For TGA measurements, samples were initially held at 150 °C to dry out the remaining water for 30 min which was followed by heating to 800 °C in an air or argon flow at a rate of 10 °C min^{-1}. TGA measurements were performed in duplicate. TEM and selected area electron diffraction of the brookite NRs were performed on an FEI Tecnai 20 electron microscope operating at 200 kV. The crystalline structures of the brookite NRs were measured by a HRTEM (FEI-Talos F200X electron microscope). Typically, at least 100 particles were counted to calculate the brookite NRs size distribution and polydispersity index. POM was performed with a Leica DM2700P microscope equipped with crossed polarizers and images were recorded with a Nikon Z6 camera.

Supporting Information

Supporting Information is available from the Wiley Online Library or from the author.

Acknowledgements

The authors acknowledge the Dutch Technology Foundation STW (grant 14176), which is part of the Netherlands Organization for Scientific Research-Applied and Engineering Sciences (NWO-TTW) and partly funded by the Ministry of Economic Affairs. X.X. acknowledges the financial support from the EU H2020-MSCA-ITN-2015 project "MULTIMAT" (project number: 676045). A.G.-C. and X.C. acknowledge the European Research Council for their support via the ERC Consolidator Grant NANO-INSITU (grant 683076). The authors would like to thank Dennie Wezendonk for the TGA/MS measurements, Peter Helfferich and Chris Schneijdenberg for technical assistance, Winnie Kong for her help with electric field experiments, Dr. Matteo Cargnello for very useful advice on synthesizing long brookite nanorods and Prof. Henk Lekkerkerker for fruitful discussions.

Conflict of Interest

The authors declare no conflict of interest.

Keywords

brookite titanium dioxide, liquid crystals, nanorods, self-assembly, surface ligands

Received: June 30, 2020
Revised: August 18, 2020
Published online:

[1] L. Yang, Z. Zhou, J. Song, X. Chen, *Chem. Soc. Rev.* **2019**, *48*, 5140.
[2] B. Liu, Y. Wu, S. Zhao, *Chem. - Eur. J.* **2018**, *24*, 10562.
[3] X. Bouju, É. Duguet, F. Gauffre, C. R. Henry, M. L. Kahn, P. Mélinon, S. Ravaine, *Adv. Mater.* **2018**, *30*, 1706558.
[4] S. Sacanna, D. J. Pine, *Curr. Opin. Colloid Interface Sci.* **2011**, *16*, 96.
[5] Z. Quan, J. Fang, *Nano Today* **2010**, *5*, 390.
[6] S. Park, H. Mundoor, B. Fleury, P. Davidson, J. van de Lagemaat, I. I. Smalyukh, *Adv. Opt. Mater.* **2019**, *7*, 1900041.
[7] B. T. Diroll, N. J. Greybush, C. R. Kagan, C. B. Murray, *Chem. Mater.* **2015**, *27*, 2998.
[8] M. Zanella, R. Gomes, M. Povia, C. Giannini, Y. Zhang, A. Riskin, M. van Bael, Z. Hens, L. Manna, *Adv. Mater.* **2011**, *23*, 2205.
[9] I. Dierking, *Liq. Cryst.* **2019**, *46*, 2057.
[10] B. Liu, T. H. Besseling, A. van Blaaderen, A. Imhof, *Phys. Rev. Lett.* **2015**, *115*, 078301.
[11] Z. Dogic, P. Sharma, M. J. Zakhary, *Annu. Rev. Condens. Matter Phys.* **2014**, *5*, 137.
[12] G. J. Vroege, H. N. W. Lekkerkerker, *Rep. Prog. Phys.* **1992**, *55*, 1241.
[13] B. Xue, T. Li, B. Wang, L. Ji, D. Yang, A. Dong, *Sustain. Energy Fuels* **2018**, *2*, 616.
[14] A. Dessombz, C. R. Pasquier, P. Davidson, C. Chanéac, *J. Phys. Chem. C* **2010**, *114*, 19799.
[15] A. Rizzo, C. Nobile, M. Mazzeo, M. De Giorgi, A. Fiore, L. Carbone, R. Cingolani, L. Manna, G. Gigli, *ACS Nano.* **2009**, *3*, 1506.
[16] A. Dessombz, D. Chiche, P. Davidson, P. Panine, C. Chanéac, J. P. Jolivet, *J. Am. Chem. Soc.* **2007**, *129*, 5904.
[17] B. Y. T. Radhakrishnan, *Proc. Indian Acad. Sci., Math. Sci.* **1951**, *35*, 117.
[18] T. R. Gordon, M. Cargnello, T. Paik, F. Mangolini, R. T. Weber, P. Fornasiero, C. B. Murray, *J. Am. Chem. Soc.* **2012**, *134*, 6751.
[19] P. Magalhães, L. Andrade, O. C. Nunes, A. Mendes, *Rev. Adv. Mater. Sci.* **2017**, *51*, 91.
[20] M. Cargnello, T. Montini, S. Y. Smolin, J. B. Priebe, J. J. D. Jaén, V. V. T. Doan-Nguyen, I. S. McKay, J. A. Schwalbe, M.-M. Pohl, T. R. Gordon, Y. Lu, J. B. Baxter, A. Brückner, P. Fornasiero, C. B. Murray, *Proc. Natl. Acad. Sci. U. S. A.* **2016**, *113*, 3966.
[21] K. Bourikas, C. Kordulis, A. Lycourghiotis, *Chem. Rev.* **2014**, *114*, 9754.
[22] M. Casavola, R. Buonsanti, G. Caputo, P. D. Cozzoli, *Eur. J. Inorg. Chem.* **2008**, *2008*, 837.
[23] M. Cargnello, T. R. Gordon, C. B. Murray, *Chem. Rev.* **2014**, *114*, 9319.
[24] C. Dinh, T. Nguyen, F. Kleitz, T. Do, *ACS Nano* **2009**, *3*, 3737.
[25] B. Wu, C. Guo, N. Zheng, Z. Xie, G. D. Stucky, *J. Am. Chem. Soc.* **2008**, *130*, 17563.
[26] B. De Nijs, S. Dussi, F. Smallenburg, J. D. Meeldijk, D. J. Groenendijk, L. Filion, A. Imhof, A. van Blaaderen, M. Dijkstra, *Nat. Mater.* **2015**, *14*, 56.
[27] F. Montanarella, J. J. Geuchies, T. Dasgupta, P. T. Prins, C. van Overbeek, R. Dattani, P. Baesjou, M. Dijkstra, A. V. Petukhov, A. van Blaaderen, D. Vanmaekelbergh, *Nano Lett.* **2018**, *18*, 3675.
[28] P. Bolhuis, D. Frenkel, *J. Chem. Phys.* **1997**, *106*, 666.
[29] M. A. Boles, D. Ling, T. Hyeon, D. V. Talapin, *Nat. Mater.* **2016**, *15*, 364.
[30] M. A. Boles, D. V. Talapin, *ACS Nano* **2019**, *13*, 5375.
[31] X. Ye, J. Chen, M. Engel, J. A. Millan, W. Li, L. Qi, G. Xing, J. E. Collins, C. R. Kagan, J. Li, S. C. Glotzer, C. B. Murray, *Nat. Chem.* **2013**,*5*, 466.
[32] M. A. Boles, D. V. Talapin, *J. Am. Chem. Soc.* **2015**, *137*, 4494.
[33] K. Bian, J. J. Choi, A. Kaushik, P. Clancy, D. M. Smilgies, T. Hanrath, *ACS Nano* **2011**, *5*, 2815.
[34] Z. Wang, C. Schliehe, K. Bian, D. Dale, W. A. Bassett, T. Hanrath, C. Klinke, H. Weller, *Nano Lett.* **2013**, *13*, 1303.
[35] B. Lee, K. Littrell, Y. Sha, E. V. Shevchenko, *J. Am. Chem. Soc.* **2019**, *141*, 16651.
[36] C. Y. Lau, H. Duan, F. Wang, C. B. He, H. Y. Low, J. K. W. Yang, *Langmuir* **2011**, *27*, 3355.
[37] B. W. Goodfellow, M. R. Rasch, C. M. Hessel, R. N. Patel, D. M. Smilgies, B. A. Korgel, *Nano Lett.* **2013**, *13*, 5710.
[38] P. S. Shah, J. D. Holmes, K. P. Johnston, B. A. Korgel, *J. Phys. Chem. B* **2002**, *106*, 2545.
[39] B. W. Goodfellow, Y. Yu, C. A. Bosoy, D. M. Smilgies, B. A. Korgel, *J. Phys. Chem. Lett.* **2015**, *6*, 2406.
[40] T. Kister, D. Monego, P. Mulvaney, A. Widmer-Cooper, T. Kraus, *ACS Nano* **2018**, *12*, 5969.
[41] S. W. Winslow, J. W. Swan, W. A. Tisdale, *J. Am. Chem. Soc.* **2020**, *142*, 39.
[42] Z. Zhang, Q. Wu, G. Johnson, Y. Ye, X. Li, N. Li, M. Cui, J. D. Lee, C. Liu, S. Zhao, S. Li, A. Orlov, C. B. Murray, X. Zhang, T. B. Gunnoe, D. Su, S. Zhang, *J. Am. Chem. Soc.* **2019**, *141*, 16548.
[43] P. P. Wang, Q. Qiao, Y. Zhu, M. Ouyang, *J. Am. Chem. Soc.* **2018**, *140*, 9095.
[44] R. Gomes, A. Hassinen, A. Szczygiel, Q. Zhao, A. Vantomme, J. C. Martins, Z. Hens, *J. Phys. Chem. Lett.* **2011**, *2*, 145.
[45] D. Wilson, M. A. Langell, *Appl. Surf. Sci.* **2014**, *303*, 6.
[46] Z. Ren, C. Chen, R. Hu, K. Mai, G. Qian, Z. Wang, *J. Nanomater.* **2012**, *2012*, 1.
[47] M. Zorn, S. Meuer, M. N. Tahir, Y. Khalavka, C. Sönnichsen, W. Tremel, R. Zentel, *J. Mater. Chem.* **2008**, *18*, 3050.
[48] S. Meuer, P. Oberle, P. Theato, W. Tremel, R. Zentel, *Adv. Mater.* **2007**, *19*, 2073.
[49] F. Cheng, E. Verrelli, F. A. Alharthi, S. M. Kelly, M. O'Neill, N. T. Kemp, S. P. Kitney, K. T. Lai, G. H. Mehl, T. Anthopoulos, *Nanoscale Adv.* **2018**, *1*, 254.
[50] M. Green, *J. Mater. Chem.* **2010**, *20*, 5797.
[51] D. Jishkariani, K. C. Elbert, Y. Wu, J. D. Lee, M. Hermes, D. Wang, A. van Blaaderen, C. B. Murray, *ACS Nano* **2019**, *13*, 5712.
[52] K. C. Elbert, D. Jishkariani, Y. Wu, J. D. Lee, B. Donnio, C. B. Murray, *Chem. Mater.* **2017**, *29*, 8737.
[53] B. T. Diroll, K. M. Weigandt, D. Jishkariani, M. Cargnello, R. J. Murphy, L. A. Hough, C. B. Murray, B. Donnio, *Nano Lett.* **2015**, *15*, 8008.
[54] D. Jishkariani, B. T. Diroll, M. Cargnello, D. R. Klein, L. A. Hough, C. B. Murray, B. Donnio, *J. Am. Chem. Soc.* **2015**, *137*, 10728.
[55] S. Meuer, K. Fischer, I. Mey, A. Janshoff, M. Schmidt, R. Zentel, *Macromolecules* **2008**, *41*, 7946.
[56] M. Zorn, S. Meuer, M. N. Tahir, W. Tremel, K. Char, R. Zentel, *J. Nanosci. Nanotechnol.* **2010**, *10*, 6845.
[57] R. Buonsanti, V. Grillo, E. Carlino, C. Giannini, T. Kipp, R. Cingolani, P. D. Cozzoli, *J. Am. Chem. Soc.* **2008**, *130*, 11223.
[58] V. Krayzman, E. Cockayne, A. C. Johnston-Peck, G. Vaughan, F. Zhang, A. J. Allen, L. Y. Kunz, M. Cargnello, L. H. Friedman, I. Levin, *Chem. Mater.* **2020**, *32*, 286.
[59] M. J. Vold, *J. Colloid Sci.* **1954**, *9*, 451.
[60] A. P. Philipse, A. M. Nechifor, C. Patmamanoharan, *Langmuir* **1994**, *10*, 4451.
[61] J. N. Israelachvili, *Intermolecular and Surface Forces: Third Edition*, Elsevier, Amsterdam, Netherlands **2011**.
[62] A. Dong, J. Chen, P. M. Vora, J. M. Kikkawa, C. B. Murray, *Nature* **2010**, *466*, 474.

[63] T. Paik, B. T. Diroll, C. R. Kagan, C. B. Murray, *J. Am. Chem. Soc.* **2015**, *137*, 6662.
[64] T. Paik, D. K. Ko, T. R. Gordon, V. Doan-Nguyen, C. B. Murray, *ACS Nano* **2011**, *5*, 8322.
[65] J. J. Geuchies, G. Soligno, E. Geraffy, C. P. Hendrikx, C. van Overbeek, F. Montanarella, M. R. Slot, O. V. Konovalov, A. V. Petukhov, D. Vanmaekelbergh, *Commun. Chem.* **2020**, *3*, 1.
[66] B. Ye, G. Qian, X. Fan, Z. Wang, *Curr. Nanosci.* **2010**, *6*, 262.
[67] D. Baranov, A. Fiore, M. van Huis, C. Giannini, A. Falqui, U. Lafont, H. Zandbergen, R. Cingolani, L. Manna, *Nano Lett.* **2010**, *10*, 743.
[68] W. Li, C. H. Hinton, S. S. Lee, J. Wu, J. D. Fortner, *Environ. Sci. Nano* **2016**, *3*, 85.
[69] Y. Liang, Y. Xie, D. Chen, C. Guo, S. Hou, T. Wen, F. Yang, K. Deng, I. I. Smalyukh, Q. Liu, *Nat. Commun.* **2017**, *8*, 1410.
[70] P. A. Buining, H. N. W. Lekkerkerker, *J. Phys. Chem.* **1993**, *97*, 11510.
[71] A. M. Bohle, R. Hołyst, T. Vilgis, *Phys. Rev. Lett.* **1996**, *76*, 1396.
[72] M. P. B. van Bruggen, J. K. G. Dhont, H. N. W. Lekkerkerker, *Macromolecules* **1999**, *32*, 2256.
[73] G. J. Vroege, A. V. Petukhov, B. J. Lemaire, P. Davidson, *Adv. Mater.* **2006**, *18*, 2565.
[74] A. Kuijk, D. V. Byelov, A. V. Petukhov, A. van Blaaderen, A. Imhof, *Faraday Discuss.* **2012**, *159*, 181.
[75] M. A. Bates, D. Frenkel, *J. Chem. Phys.* **1998**, *109*, 1208.
[76] R. van Roij, P. Bolhuis, B. Mulder, D. Frenkel, *Phys. Rev. E* **1995**, *52*, R1277.
[77] B. S. John, C. Juhlin, F. A. Escobedo, *J. Chem. Phys.* **2008**, *128*, 044909.
[78] Y. Zhang, F. M. Liu, *Appl. Surf. Sci.* **2016**, *367*, 559.
[79] L. S. Li, A. P. Alivisatos, *Adv. Mater.* **2003**, *15*, 408.
[80] R. Piazza, *Rep. Prog. Phys.* **2014**, *77*, 056602.
[81] S. V. Savenko, M. Dijkstra, *Phys. Rev. E: Stat. Phys., Plasmas, Fluids, Relat. Interdiscip. Top.* **2004**, *70*, 51401.
[82] P. Prinsen, P. van der Schoot, *Phys. Rev. E: Stat. Phys., Plasmas, Fluids, Relat. Interdiscip. Top.* **2003**, *68*, 11.
[83] I. Niezgoda, J. Jaworska, D. Pociecha, Z. Galewski, *Liq. Cryst.* **2015**, *42*, 1148.
[84] A. van Blaaderen, M. Dijkstra, R. van Roij, A. Imhof, M. Kamp, B. W. Kwaadgras, T. Vissers, B. Liu, *Eur. Phys. J. Spec. Top.* **2013**, *222*, 2895.